Applied Catalysis B: Environmental 174–175 (2015) 1–12

Contents lists available at ScienceDirect

Applied Catalysis B: Environmental

journal homepage: www.elsevier.com/locate/apcatb

Bifunctional $Mo_3VO_x/H_4SiW_{12}O_{40}/Al_2O_3$ catalysts for one-step conversion of glycerol to acrylic acid: Catalyst structural evolution and reaction pathways

Licheng Liu, Bo Wang*, Yonghua Du, Ziyi Zhong, Armando Borgna

*Institute of Chemical and Engineering Sciences, A*STAR (Agency for Science, Technology and Research), 1 Pesek Road, Jurong Island, Singapore 627833, Singapore*

ARTICLE INFO

Article history:
Received 18 November 2014
Received in revised form 23 January 2015
Accepted 25 February 2015
Available online 26 February 2015

Keywords:
Bifunctional catalyst
Oxydehydration
Glycerol
Acrylic acid
Acrolein

ABSTRACT

A series of $Mo_3VO_x/H_4SiW_{12}O_{40}/Al_2O_3$ catalysts were prepared and applied to one-step oxydehydration of glycerol to acrylic acid. The catalysts were thoroughly characterized by BET, XRD, TEM, TGA, NH_3-TPD, and XAFS techniques. It was found that acetic acid was produced in parallel with acrylic acid with similar yield when adjusting Mo_3VO_x content in the catalysts. Increasing calcination temperature from 350 to 650 °C led to structural evolution of supported active species and subsequent activity change. Crystallinity of Mo_3VO_x increased with calcination temperature and a large amount of $(V,Mo)O_x$ hetero-polyoxo mixed oxides were formed above 550 °C. The Keggin structure of $H_4SiW_{12}O_{40}$ began to dissociate around 450 °C causing the formation of various WO_x species. Above 450 °C, the yield of acrylic acid dropped while that of acrolein could reach its maximum value with increase of the catalyst calcination temperature. In contrast, the yield of acetic acid showed a minor change always. Based on the catalytic and characterization results, possible active centers and reaction pathways are thus proposed, and for the improvement of the bifunctional catalyst for the one-step conversion of glycerol, both the acidic and redox properties of catalysts should be finely tuned. This work provides new insight into the reaction mechanism and the catalyst design for the one-step oxydehydration of glycerol to acrylic acid.

© 2015 Elsevier B.V. All rights reserved.

1. Introduction

Glycerol is one of the potential bio-derived building blocks for biorefinery [1–3], and also a major by-product in the production of biodiesel via transesterification of vegetable oil or animal fat with an alcohol [4–6]. Generally, 10 kg of glycerol can be produced with production of every 100 kg of biodiesel [5,7]. Glycerol gluts in market in recent years. Intensive efforts were made to convert glycerol to other value-added chemicals, such as hydrogenolysis to 1,3-propanediol [8–10], reforming to hydrogen [11–13], oxidation to glyceric acid [14–16], etc.

Acrylic acid and its derived esters are important bulk chemicals with broad application in the polymer industry for production of super-absorbers, fabrics, adhesives and paints, etc. [17–19]. In industry, acrylic acid is produced by a two-step propene oxidation process [20,21]. In the first step, propene is selectively oxidized with air to acrolein on Bi/Mo-catalysts, then acrolein is further oxidized to acrylic acid on Mo/V/W-mixed oxides catalyst. Because of the rising price of propylene and abundance of glycerol supply, the dehydration of glycerol to acrolein becomes a competitive route to produce acrolein and acrylic acid [22–24].

The gaseous dehydration of glycerol to acrolein has been widely studied on various solid acid catalysts, such as zeolites, heteropoly acids and WO_3–ZrO_2 catalysts [25–46], and it is reported that the physical structure, acidic strength and active species of catalyst affect the dehydration activity. In contrast, the second step, the selective oxidation of acrolein to acrylic acid, is rarely mentioned in recent literature as it is considered as a mature industrial process. Vogel and co-workers performed some fundamental research on Mo–V–W based catalysts for this partial oxidation reaction [21,47–50]. They found that the increase in selectivity of acrylic acid is directly connected to the formation of the nanocrystalline MoO_3–Mo_5O_{14} type oxide system. The triclinic V_2O_5 type oxide may mainly be responsible for the total oxidation at reaction temperatures higher than 400 °C.

Theoretically, one-step conversion of glycerol to acrylic acid is preferred as it is more economically viable than two-step conversion. However, it is difficult to obtain high acrylic acid yield

* Corresponding author. Tel.: +65 67963825; fax: +65 63166182.
E-mail address: wang_bo@ices.a-star.edu.sg (B. Wang).

http://dx.doi.org/10.1016/j.apcatb.2015.02.032
0926-3373/© 2015 Elsevier B.V. All rights reserved.

because it requires bi-functional catalyst suitable for both dehydration and oxidation simultaneously. So far very limited success has been achieved in this aspect. Deleplanqe et al. and Soriano et al. studied this reaction by using Mo–V–O and W–V–O catalysts, respectively [22,51], and obtained ca. 20% acrylic acid yield in the two cases, whereas CO_x(CO/CO_2) still remained as the major complete oxidation product. Recently, Wang et al. reported the catalytic oxidative dehydration of glycerol over a catalyst with iron oxide domains embedded in an iron orthovanadate phase, the best acrylic acid yield was 14% but with more acetic acid as co-product [52]. Comparatively, a W–V–Nb mixed oxide catalyst with a hexagonal tungsten bronze structure showed rather high acrylic acid yield (maximum 50.5%) in the one-pot glycerol oxidehydration to acrylic acid reaction, reported by Chieregato et al. [53,54]. However, the catalyst properties and catalytic mechanism are still not well described, which may contribute to design new catalyst to the reaction. Actually, the two-step in single reactor with double catalyst bed configuration, by loading dehydration and oxidation catalysts sequentially, is more efficient in conversion of glycerol to acrylic acid in some extent [55]. The comparison would be also provided in this work.

$H_4SiW_{12}O_{40}$ and Mo_3VO_x are well-proved active species for dehydration of glycerol and oxidation of acrolein, respectively [19,21,30,53,56–58]. In this work, to understand the mechanism and achieve one-step conversion of glycerol to acrylic acid, we synthesized and tested a series of $Mo_3VO_x/H_4SiW_{12}O_{40}/Al_2O_3$ bi-functional catalysts, in which, heteropoly acid $H_4SiW_{12}O_{40}$ acts as the dehydration component, while Mo_3VO_x mixed oxides as the oxidation component. Usually, the active centers are generated in the calcination process. Therefore, the evolution of reactive phases with calcination temperature is investigated, and is correlated with the catalytic property changes. This work not only provides insights into the active sites in these bi-functional catalysts and reaction pathways, but also shed lights on designing and development of better catalysts.

2. Experimental

2.1. Catalyst synthesis

Commercial Al_2O_3 (Aldrich, 150 mesh) was used as support without further purification. $H_4SiW_{12}O_{40}/Al_2O_3$ was firstly prepared by wet impregnation method. Typically, 3.0 g of tungstosilicic acid hydrate (Aldrich) was dissolved in 20 ml DI water under stirring. Then 7.0 g of Al_2O_3 was added to the above solution and stirring continued overnight. The mixture was dried at 110 °C in oven prior to further use. The Mo_3VO_x mixed oxides were synthesized by the hydrothermal method. In details, 5.88 g of $(NH_4)_6Mo_7O_{24}{\cdot}4H_2O$ (Sigma–Aldrich) and 2.18 g of $VOSO_4$ (Aldrich) were dissolved in 80 ml of DI water under stirring. The precursor solution was transferred to a stainless steel autoclave equipped with a 100 ml Teflon lined tube. Hydrothermal reaction of the liquid (mole ratio: Mo/V = 3/1) was carried out for 36 h. The obtained gray solid was washed with DI water and dried at 120 °C. Then the desired amount of $H_4SiW_{12}O_{40}/Al_2O_3$ and Mo_3VO_x was mixed in water/ethanol (6/1 in volume) to prepare $Mo_3VO_x/H_4SiW_{12}O_{40}/Al_2O_3$ catalysts. The weight ratio of Mo_3VO_x and $H_4SiW_{12}O_{40}/Al_2O_3$ varied by 1/1, 1/1.5, 1/2, 1/5. After stirring overnight and drying, the catalysts were calcined at 350 °C for 4 h in air. The catalyst with 1/1.5 ratio was also calcined at 450, 550, 650 °C additionally for comparison. The Mo_3VO_x catalyst was calcined at 350 and 450 °C separately and used as oxidation catalyst in the reaction with a double catalyst bed configuration. The $H_4SiW_{12}O_{40}$, $H_4SiW_{12}O_{40}/Al_2O_3$, Mo_3VO_x and $Mo_3VO_x/H_4SiW_{12}O_{40}/Al_2O_3$ were abbreviated as HSiW, SiW/Al_2O_3, Mo_3VO_x and $MoV/SiW/Al_2O_3$, respectively, in the text.

2.2. Characterizations

N_2 adsorption/desorption isotherms were determined on a physical adsorption apparatus (Micromeritics, ASAP 2420). The samples were pretreated at 300 °C under vacuum for 5 h before measurements. Calculations of the specific surface area (BET), pore volume, and average pore size (BJH method) were performed with the software of the apparatus.

X-ray diffraction (XRD) patterns of the catalysts were recorded on an X-ray diffractometer (Bruker AXS D8 Focus) equipped with a Cu Kα source (λ = 1.5406 Å) operated at 40 kV and 40 mA. The crystalline phases were identified by comparing with reference patterns available in the JCPDS database.

The transmission electron microscope (TEM) images were recorded on Tecnai TF 20 S-twin with Lorentz lens operating at 200 kV. The catalyst powder was dispersed in ethanol by sonication. A drop of suspension was deposited on a carbon coating copper grid before TEM examination.

The temperature-programmed desorption of NH_3 (NH_3-TPD) was carried out over 0.10 g of sample from 30 to 850 °C at a heating rate of 10 °C/min while monitoring the thermal conductivity detector (TCD) signals (Thermo TPD/R/O 1100) after saturation with NH_3 at 100 °C for 30 min and then purged with He at 30 °C for 1 h. The sample was treated in He at 300 °C for 1 h before the TPD experiment. The TPD curves were analyzed, with a multiple Gaussian function for fitting and the area of each peak was calculated by Origin 7.5. The peak area can be correlated with the amount of adsorbed NH_3 based on the pulsed NH_3 injection experiment.

Thermal analysis (TG-DTA) was conducted on thermogravimetric analyzer (TGA Q500). The sample was placed in a α-Al_2O_3 holder and heated in flowing air (50 ml min^{-1}) from room temperature to 800 °C at a rate of 10 °C min^{-1}.

X-ray absorption spectra of W-L_3 edge was recorded at the XAFCA beam line at Singapore Synchrotron Light Source (SSLS). A Si (1 1 1) two crystal monochromator was used. Ion chambers filled with N_2 (85%)/Ar (15%) and N_2 (50%)/Ar (50%) were used for I_0 and I detection, respectively. The energy was calibrated by using a Pt foil. The data reduction was performed by the Athena 0.8.056 program (by Bruce Ravel).

2.3. Catalytic activity test

Glycerol oxydehydration reactions were conducted in a vertical fixed-bed reactor under atmospheric pressure. A quartz tube reactor with an internal diameter of 7 mm was used. One gram of catalyst was palletized and sieved to sizes between 250 and 400 microns and loaded in the middle section of the reactor, with quartz wool packed at both ends. For double catalyst bed reaction in one reactor, 0.5 g of SiW/Al_2O_3 and 0.5 g of Mo_3VO_x catalyst were loaded sequentially and separated by quartz wool. Also, 0.5 g of SiW/Al_2O_3 and 0.5 g of Mo_3VO_x catalyst (250 and 400 μ) were mechanically mixed and loaded to reactor to test the activity. Before reaction, the catalyst was pretreated at 300 °C for 1 h in N_2 with a flow rate of 25 ml min^{-1}. Aqueous glycerol solution (20% w/w) was fed by a syringe pump. The composition of the feed gas was $N_2/O_2/H_2O$/glycerol = 59.0:4.2:35.1:1.7 (molar ratio), which composes N_2 = 25 ml min^{-1}, 20 vol% O_2/N_2 = 15 ml min^{-1}, 20 wt% glycerol/H_2O = 1.5 ml h^{-1}. The products were collected in 10 ml of water in a cold trap directly connected to the outlet of the reactor. A second cold trap with 40 ml of water in an ice-bath was placed after online GC to further condense low boiling compounds. 25 μl of 2-butanol, as internal standard, was mixed with 1 ml of products in water in each trap and quickly analyzed by GC (Shimadzu 2014, Japan) with an auto-sampler equipped with a capillary column (Phenomenex, ZB-WAX, 60m × 0.25mm × 0.5 μm) and a flame ionization detector (FID). The chromatography column was run at a

program from 60 °C to 240 °C at a ramping rate of 10 °C min min^{-1} and kept at 240 °C for 12 min. The N_2, O_2, CO and CO_2 in gas phase were analyzed by online GC (Varian CP-3800) with two columns of 5 A molecular sieve and Porapak Q.

The results of all GC analyses for liquid- and gas-phases were collated to evaluate the conversion, selectivity, and carbon balance. Glycerol conversion was found to be 100% for all reactions. The conversion of oxygen (X_{oxy}, mol%) was determined using online GC by measuring the integration area ratios of oxygen to nitrogen for the inlet and outlet gases. Product selectivity (S_i, mol%) was calculated from the molar concentrations of product and glycerol according to Eq. (1)

$$S_i = \frac{M_i}{M_{gly,in} - M_{gly,out}} \times \frac{z_i}{3} \times 100 \quad (1)$$

where z represents the number of carbon atoms, for example, $z = 3$ for acrylic acid and $z = 2$ for acetic acid. M_i represents the detected molar quantity of product i [24].

3. Results

3.1. Catalytic reaction results

The catalytic oxydehydration of glycerol over Al_2O_3, SiW/Al_2O_3 and $MoV/SiW/Al_2O_3$ (calcined at 350 °C) catalysts was investigated and the results are presented in Table 1. Under the oxidation reaction condition, Al_2O_3 showed a total glycerol conversion yielding a wide range of oxy-containing products. Acrolein had a 22.5% of selectivity as the main product. When HSiW was supported on Al_2O_3, the selectivity to acrolein was improved to 54.3%. No acrylic acid was detected in the products on both catalysts. The reaction was likely to be dehydrated under aerobic condition. In contrast, Tsukuda et al. investigated the glycerol dehydration activity over Al_2O_3 and SiW/Al_2O_3 catalysts, and obtained 37% and 74% selectivity of acrolein with 98% and 100% glycerol conversion respectively at a reaction temperature of 325 °C [33]. The introduction of Mo_3VO_x to SiW/Al_2O_3 led to a sharp drop of acrolein selectivity to 2.9%. In the meantime, a selectivity of 12.1% to acrylic acid and 11.9% to acetic acid were observed. CO and CO_2 were the by-products with yields as high as 36.5% and 19.1%, respectively.

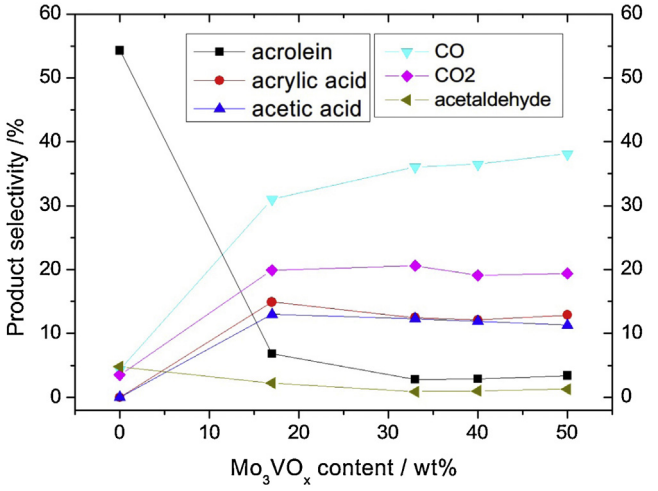

Fig. 1. Catalytic results on $MoV/SiW/Al_2O_3$ with different Mo_3VO_x content. The catalysts were all calcined at 350 °C in air. Reaction conditions: 1.0 g catalyst loading, 300 °C, 0.1 MPa. Feeding N_2:O_2:H_2O:glycerol = 59.0:4.2:35.1:1.7 in molar ratio. Reaction time was 2 h.

The conversion of oxygen was over 70% on the $MoV/SiW/Al_2O_3$ catalysts. The carbon balance was usually higher than 80% (except on Al_2O_3), and the rest of carbon was in the form of coke and other unknown heavy compounds [24,51]. Similarly, the oxygen balance was lower than 100%, due to the incorporation of oxygen into the undetected heavy compounds.

To further alter the Mo_3VO_x content in the catalysts, the weight ratio of Mo_3VO_x to SiW/Al_2O_3 was adjusted to 1/5, 1/2, 1/1.5, 1/1. All catalysts were calcined at 350 °C. The catalytic results are shown in Fig. 1. The selectivity to acrylic acid and acetic acid was parallel and showed a little drop with increase of the Mo_3VO_x content. The selectivity to acrolein had a sharp decrease to less than 10% with initial Mo_3VO_x introduction and then dropped slowly. The CO selectivity increased with Mo_3VO_x content, while trend of CO_2 selectivity was similar to acrylic acid. The CO/CO_2 composed of main by-products. Another product was acetaldehyde, which had a selectivity lower than 5% and decreased with Mo_3VO_x. The detected

Table 1
Catalytic results of glycerol conversion over Al_2O_3, SiW/Al_2O_3, and $MoV/SiW/Al_2O_3$ in one step and SiW/Al_2O_3 & Mo_3VO_x in two catalyst bed as well as mechanically mixed configuration.

Catalyst	Al_2O_3	SiW/Al_2O_3	$MoV/SiW/Al_2O_3$[a]	SiW/Al_2O_3 and Mo_3VO_x (350 °C)[b]	SiW/Al_2O_3 and Mo_3VO_x (450 °C)[b]	SiW/Al_2O_3 and Mo_3VO_x (450 °C)[c]
$X_{glycerol}$[d]	100	100	100	100	100	100
X_{oxy}[e]	27	15	76	28	66	79
Selectivity (=yield) (%)						
Acrolein	22.5	54.3	2.9	35.2	3.0	0.9
Acrylic acid	0	0	12.1	19.8	46.2	9.0
Acetic acid	1.2	0	11.9	5.5	11.1	12.5
Acetaldehyde	9.0	4.8	1.0	3.7	0	0.2
Formaldehyde	5.8	0	0	1.2	0.2	0.3
Hydroxyacetone	2.6	1.4	0	0	0	0
Propionaldehyde	2.1	1.1	0	0	0	0
Acetone	2.6	15.4	0	0	0.1	0
CO	6.9	4.3	36.5	4.3	18.8	52.6
CO_2	12.4	3.5	19.1	6.7	14.3	20.0
Oxygen balance	71	62	66	86	79	72
Carbon balance	68	85	84	77	94	96

Reaction conditions: 1.0 g catalyst loading (0.5 and 0.5 g for double catalyst bed), 300 °C, 0.1 MPa. Feeding N_2:O_2:H_2O:glycerol = 59.0:4.2:35.1:1.7 in molar ratio. Reaction time was 2 h.

[a] Calcined at 350 °C for 4 h.
[b] Double catalyst bed reaction in one reactor, calcination temperature of Mo_3VO_x catalyst in bracket.
[c] Physically mixed.
[d] Conversion of glycerol.
[e] Conversion of oxygen.

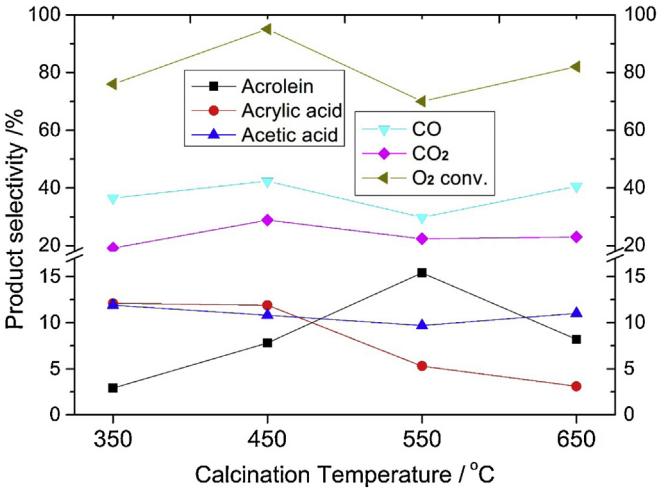

Fig. 2. Catalytic results on MoV/SiW/Al_2O_3 calcined at different temperature. The weight ratio of Mo_3VO_x to SiW/Al_2O_3 was 1/1.5. Reaction conditions: 1.0 g catalyst loading, 300 °C, 0.1 MPa. Feeding N_2:O_2:H_2O:glycerol = 59.0:4.2:35.1:1.7 in molar ratio. Reaction time was 2 h.

products (acrylic acid, acetic acid, acrolein, etc) and some undetected heavy compounds were deeply oxidized to CO (not CO_2 from the figure) with increase of Mo_3VO_x. The increasing content of Mo_3VO_x contributes to deep oxidation mostly. On the other hand, the relatively weak selectivity of Mo_3VO_x part calcined at 350 °C can not convert acrolein to acrylic acid totally, by referring the double catalyst bed results below.

The catalyst with 1/1.5 ratio of Mo_3VO_x to SiW/Al_2O_3 was also calcined at 450, 550 and 650 °C respectively and corresponding activities were measured. As shown in Fig. 2, selectivity to acrylic acid was similar over the catalysts calcined at 350 and 450 °C, but dropped sharply for the catalysts calcined at higher temperature of 550 and 650 °C. In contrast, less change happened for selectivity to acetic acid with varying calcination temperature of the catalyst. The selectivity to acrolein increased up to 15.4% till 550 °C and then dropped to 8.2% for the catalyst calcined from 350 to 650 °C.

In the one-step conversion of glycerol to acrylic acid, CO and CO_2 are usually produced in a large amount as by-products. Deleplanque et al. reported 35–45% CO_x yields in the oxydehydration of glycerol with molybdenum/tungsten vanadium based catalysts [22]. A great amount of CO and CO_2 production over tungsten–vanadium mixed oxides was also observed by Soriano et al. for the same reaction [51]. In present investigation, usually selectivity of 20–30% of CO_2 and 30–40% of CO were produced in the reaction (Fig. 2). Conversion of O_2 was higher than 70% and the highest value as high as 95% was observed on the MoV/SiW/Al_2O_3 catalyst calcined at 450 °C.

For comparison, we also separated the catalyst to dehydration and oxidation catalyst and run the reaction in double bed with consecutive packing of the catalysts. The oxidation catalyst (Mo_3VO_x) was placed directly after the dehydration catalyst (SiW/Al_2O_3). The reaction results are shown in Table 1. For Mo_3VO_x calcined at 350 °C, the reaction produced 35.2% of acrolein yield and 19.8% of acrylic acid yield. The CO_x yields were much lower than that in the one-step reaction. These results suggest that Mo_3VO_x calcined at 350 °C is not active enough to convert acrolein to acrylic acid. However, when the calcination was increased to 450 °C, yield to acrylic acid could reach 46.2% while only 3.0% of acrolein remained. Spontaneously, the yields of CO_x increased to 18.8% and 14.3% dramatically, in comparison with using Mo_3VO_x calcined at 350 °C. For further exploring the effect of dehydration and oxidation catalyst configuration, the Mo_3VO_x (450 °C) and SiW/Al_2O_3 (250 and 400 microns both) were mechanically mixed to load to reactor and catalyze glycerol

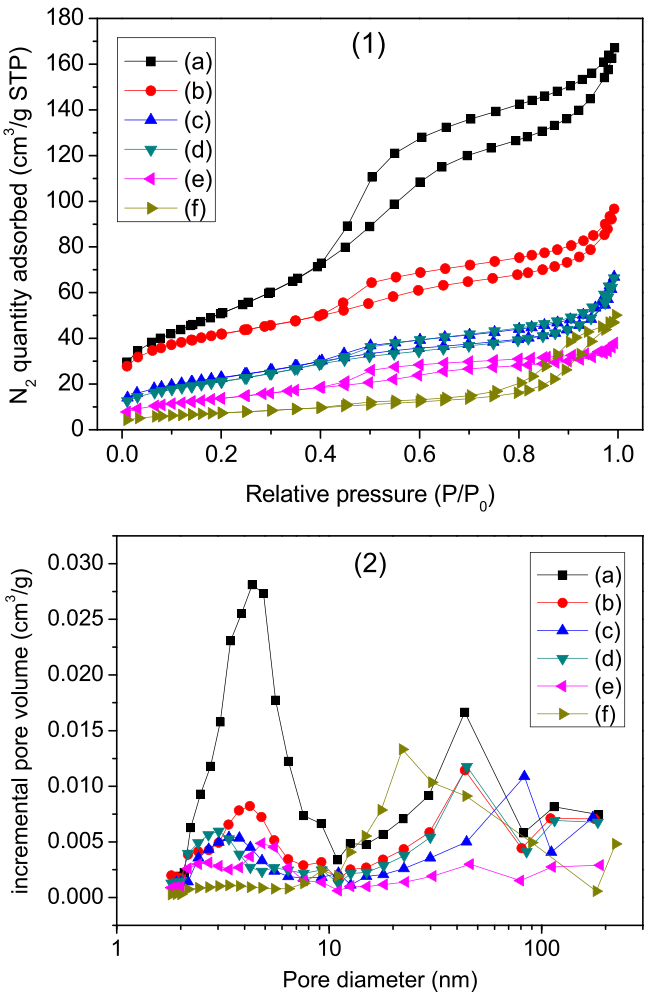

Fig. 3. N_2 adsorption–desorption isotherms (1) and pore diameter distribution curves (2). (a) Al_2O_3, (b) SiW/Al_2O_3 and MoV/SiW/Al_2O_3 calcined at (c) 350, (d) 450, (e) 550, and (f) 650 °C.

conversion to acrylic acid. The reaction result was also shown in Table 1. In this manner, the result was similar to that on MoV/SiW/Al_2O_3 catalyst calcined at 350 °C in Table 1, with a little lower acrylic acid yield and higher CO selectivity.

3.2. Characterizations

The porous structure of the catalysts calcined at different temperatures was measured by N_2 adsorption–desorption method. The N_2 adsorption–desorption isotherms and pore diameter distributions are shown in Fig. 3, and the BET surface area, average pore size and pore volume are summarized in Table 2. The N_2 adsorption–desorption isotherm of the Al_2O_3 support has a steep adsorption increase at P/P_0 = 0.4–0.6 and a hysteresis loop between adsorption and desorption curves, characteristic of type IV isotherm and suggested mesoporous structure. The loading of HSiW to Al_2O_3 led to significant decrease of N_2 quantity adsorbed due to the possible blocking or covering of some meso-pores in Al_2O_3, but the mesoporous structure still remained as the hysteresis loop still existed. Regarding the MoV/SiW/Al_2O_3 catalysts calcined at different temperatures, the N_2 quantity adsorbed showed further decrease with ramping of the temperature. The catalysts calcined at 350 and 450 °C had almost the same isotherm while the catalyst calcined at 550 °C showed similar isotherm suggesting mesoporous structure, but with reduced pore volume as the N_2 adsorption quantity became lower. The relative pressure (P/P_0) of the

Table 2
Results summarized from BET and NH_3-TPD.

Catalyst	BET			NH_3-TPD		
	Surface area ($m^2\ g^{-1}$)	Pore size (nm)	Pore volume ($cm^3\ g^{-1}$)	Peak[b] (°C)	NH_3(des)[c] ($\mu mol\ g^{-1}$)	Total ($\mu mol\ g^{-1}$)
Al_2O_3	187.2	5.4	0.251	274	69	69
SiW/Al_2O_3	145.1	3.9	0.143	278	283	283
$MoV/SiW/Al_2O_3$ (350[a])	81.9	4.6	0.095	340/420/434	110/59/232	401
$MoV/SiW/Al_2O_3$ (450[a])	77.2	5.0	0.096	280/565	49/282	331
$MoV/SiW/Al_2O_3$ (550[a])	50.6	4.4	0.056	354/583	48/40	88
$MoV/SiW/Al_2O_3$ (650[a])	26.7	10.9	0.073	410	42	42

[a] Calcination temperature (°C).
[b] NH_3 desorption temperature peak centre based on fitting result. The TPD curve may include 1–3 peaks.
[c] NH_3 desorption amount based on fitting result.

adsorption branch and the hysteresis loop moved to a value as high as 0.8 for the catalyst calcined at 650 °C, suggesting the expansion of pores. The BJH pore diameter distribution curves are shown in Fig. 3(2). For most cases, hierarchical pores distributed between 5 and 50 nm. The introduction of HSiW almost did not change the pore diameter center of Al_2O_3, indicating that HSiW molecules were mostly covered on the surface due to their large size. The supporting of Mo_3VO_x made the pore diameter decrease to 3–4 nm, for the catalysts calcined at 350 and 450 °C. It is attributed to the coverage of Mo_3VO_x on the inner surface of Al_2O_3 pores. The calcination at 550 °C led to formation of new hierarchical pores of 3 and 6 nm instead of 5 nm. After calcined at 650 °C, pores with diameter less than 5 nm disappeared while pores around 15 nm were constructed. This resulted in the change of N_2 adsorption isotherm. As shown in Table 2, the BET surface area of fresh Al_2O_3 is 187.2 $m^2\ g^{-1}$. After loading with HSiW, it became 145.1 $m^2\ g^{-1}$. With increase of the calcination temperature, it became gradually smaller. Similar trend for the pore volume change is observed.

The crystalline phase of catalysts was studied by XRD and the patterns are shown in Fig. 4. The crystalline degree of Al_2O_3 is low but the structure can still be identified as cubic symmetry of γ-Al_2O_3 (JCPDS 04-0880). The loading of HSiW further reduced the diffraction intensity of Al_2O_3 but no diffraction peak assigned to HSiW is observed, suggesting the high-dispersion of HSiW [59]. The introduction of Mo_3VO_x and calcination at 350 °C didnot arouse any peaks except a small sharp one at 22.2^0, which is assigned to (0 0 1) diffraction of $(V_{0.07}Mo_{0.93})_5O_{14}$ (JCPDS 31-1437). After calcination at 450 °C, more peaks with low intensity appeared, which were identified as mixed phases of MoO_3 (JCPDS 05-0508) and $(V_{0.07}Mo_{0.93})_5O_{14}$ (JCPDS 31-1437). The catalysts calcined at 550 and 650 °C produced much more diffraction peaks with exactly the same diffraction angles, suggesting the same crystal phase composed. The peak intensity was higher for sample calcined at 650 °C due to the growth of grain size at higher temperature. These crystallized catalysts consisted of a complex composition of various hetero-polyoxo-Mo/V/W agglomerates, each of which contributed to the recorded diffraction pattern [48]. The following phases were confirmed to be present in both catalysts, including orthorhombic WO_3 (JCPDS 20-1324), V_2O_5 (JCPDS 53-0538), triclinic $(V, Mo)_2O_5$ [21], orthorhombic Mo_4O_{11} (JCPDS 05-0337), $(V, Mo)_4O_{11}$, monoclinic VO_2 (JCPDS 65-7960) [60], etc. To compare the catalysts between one-step and double bed reaction, the XRD of Mo_3VO_x was measured and presented in Fig. S1. The as-synthesized Mo_3VO_x (without calcination) and sample calcined at 350 °C showed the same XRD diffraction peaks, which were assigned as hexagonal $(V, Mo)O_3$ species or ammonium molybdate. The crystal structure of Mo_3VO_x calcined at 450 °C transformed totally which corresponds to orthorhombic $(V, Mo)O_3$ species. Additionally, weak peaks assigned to $(V_{0.07}Mo_{0.93})_5O_{14}$ were also observed.

The NH_3-TPD was performed from 50 to 850 °C to study the acidic properties of the catalysts. The amount and strength of acidity are described as amount and temperature of NH_3 desorbed derived from multi-peak fitting (Table 2). Al_2O_3 showed a wide peak between 200 and 650 °C, suggesting the co-existence of weak, medium and strong acidic sites [61]. The strength of acidic sites is classified according to the desorption temperature as weak (150–300 °C), medium (300–500 °C), and strong (500–650 °C) [59]. Loading of HSiW to Al_2O_3 increased the number of acidic sites dramatically from 69 to 283 μmol/g. This is not consistent with Atia and Martin's results, because they observed unchanged acidity after modification of Al_2O_3 with HSiW [30,59]. A relatively lower loading

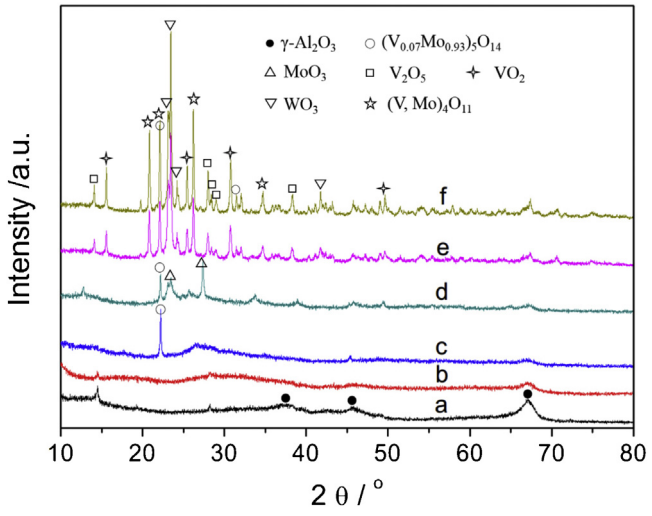

Fig. 4. XRD patterns of (a) Al_2O_3, (b) SiW/Al_2O_3 and $MoV/SiW/Al_2O_3$ calcined at (c) 350, (d) 450, (e) 550, and (f) 650 °C.

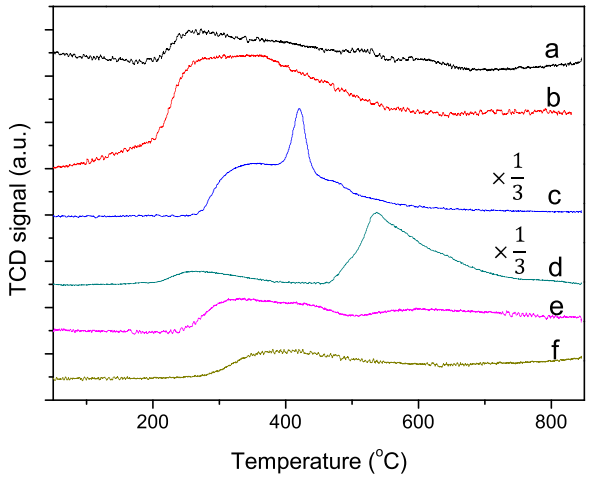

Fig. 5. NH_3-TPD profiles of (a) Al_2O_3, (b) SiW/Al_2O_3 and $MoV/SiW/Al_2O_3$ calcined at (c) 350, (d) 450, (e) 550, and (f) 650 °C.

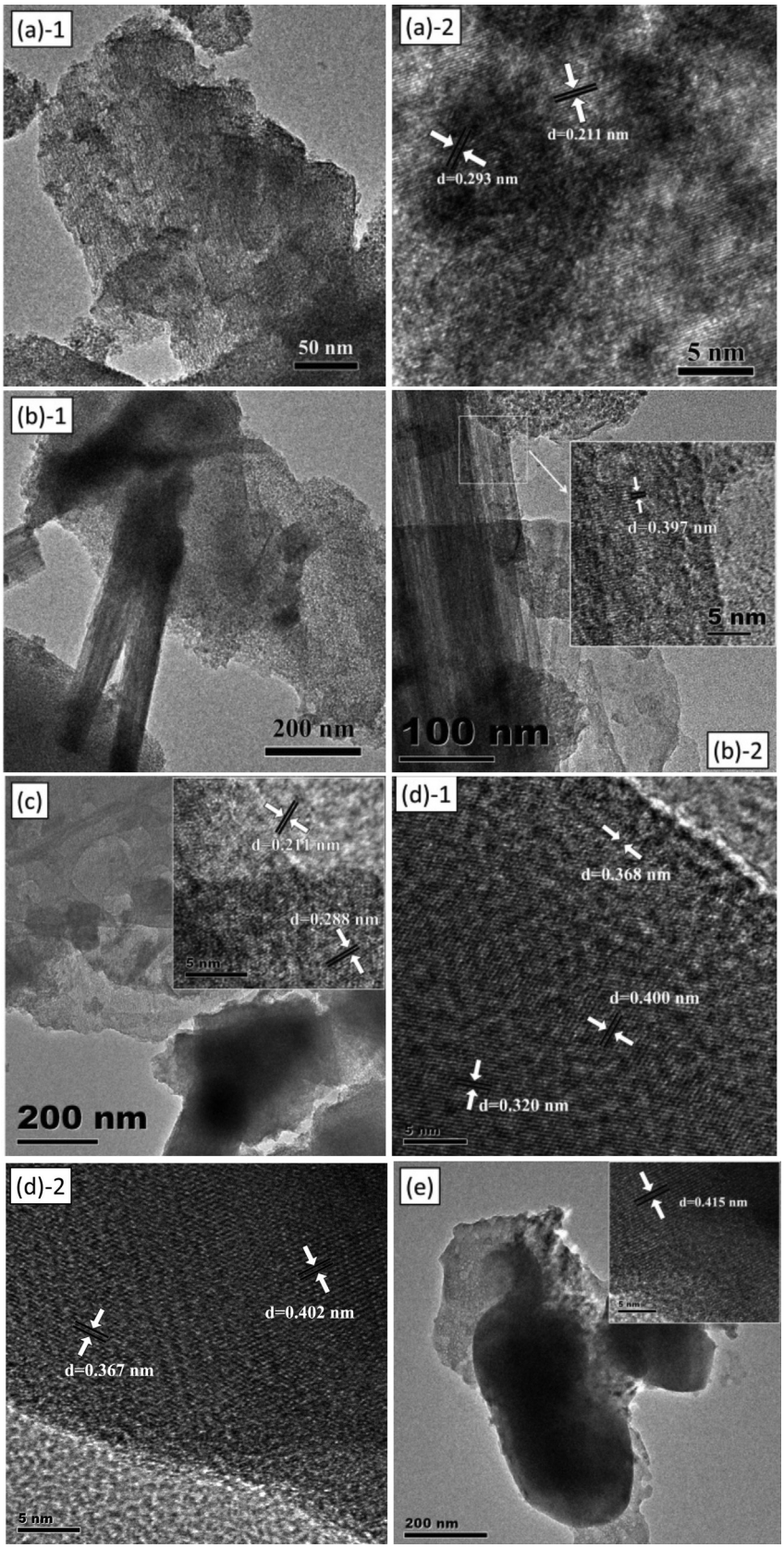

Fig. 6. TEM images of (a) SiW/Al_2O_3 and $MoV/SiW/Al_2O_3$ calcined at (b) 350, (c) 450, (d) 550, and (e) 650 °C.

of HSiW (20 wt%) and calcination under airflow in their experiment may account for the difference. After mixing SiW/Al_2O_3 with Mo_3VO_x and calcining the mixture at 350 °C, only medium acidity remained and represented by the peaks at 300–550 °C, accompanying with appearance of a sharp peak around 420 °C. The total quantity of acidity increased to 401 μmol/g. Calcination at 450 °C produced a much stronger acidity of 282 μmol/g with desorption peak centered at 565 °C. For the catalysts calcined at 550 and 650 °C, only a very small amount of weak-medium acidity remained and the medium acidic sites quantity was 88 and 42 μmol/g, respectively (Fig. 5).

The micro-structure and morphology of catalysts was studied with TEM. The porous structure of Al_2O_3 can be seen in TEM image of SiW/Al_2O_3 in Fig. 6(a)-1. HSiW was highly dispersed on the surface of Al_2O_3 with different thickness, indicated by different contrasts. From the high-resolution image of Fig. 6(a)-2, distinct crystal fringes with a spacing of 0.211 nm are observed, corresponding to *d*-spacing of Al_2O_3 (3 2 1) crystal planes. In one thick part, the lattice expansion to 0.293 nm may be ascribed to HSiW crystallines. Fig. 6(b) shows the images of $MoV/SiW/Al_2O_3$ catalyst calcined at 350 °C. The acicular nano-structure is observed besides the porous SiW/Al_2O_3 components, which is believed to be Mo_3VO_x mixed oxides. In the enlarged TEM image (Fig. 6(b)-2), *d*-spacing of crystal lattice of acicular crystal is measured to be 0.397 nm, which is assigned to $(V_{0.07}Mo_{0.93})_5O_{14}$ (0 0 1) crystal planes. But these fringes are not well-defined due to poor crystallinity. Increasing calcination temperature to 450 °C led to growth of Mo_3VO_x crystals. The lattices of Al_2O_3 and $(V,Mo)_2O_5$ are observed, which are at 0.211 nm (3 2 1) and 0.288 nm (1 1 1), respectively, in the inset zoomed image. Calcination at 550 and 650 °C resulted in fine crystallinity analyzed from the above XRD patterns. More ordered crystal fringes are shown in the high-resolution TEM images in Fig. 6(d). The *d*-spacing of 0.320 nm in Fig. 6(d)-1 is assigned to V_2O_5 (1 0 1) lattice space, that of 0.400 nm in Fig. 6(d)-1 and 0.402 nm in Fig. 6(d)-2 to $(V, Mo)_4O_{11}$ (2 1 1) crystal lattice, and that of 0.368 and 0.367 nm in Fig. 6(d)-1 and (d)-2 to WO_3 (2 0 0) lattices, but some of them are not in good crystalinity. Similarly, the *d*-spacing of 0.415 nm in Fig. 6(e) is also assigned to $(V, Mo)_4O_{11}$ (0 1 1) crystal plane space with many V atoms in crystal lattice. The diameter of Mo_3VO_x crystal grew to about 200 nm after calcination at 650 °C.

Thermogravimetric (TG) analysis was applied to evaluate the thermal stability of bulk HSiW and supported SiW/Al_2O_3, as well as $MoV/SiW/Al_2O_3$ (Fig. 7). Three weight loss peaks are observed in the DTG curve of HSiW and the percentage of weight loss is 0.99%, 3.45% and 1.13%, respectively. The first two peaks are due to the loss of physisorbed water and removal of water from hydrated heteropoly acid [59,62]. The third peak above 450 °C may relate to the decomposition of HSiW to a new compound of WO_3(Si), which can be considered as a solid solution of silicon in WO_3 [59]. Contrarily, the weight loss of SiW/Al_2O_3 is almost continuous from the low temperature. The DTG peaks are not sharp but still can be distinguished. The weight loss at relatively low temperature can also be assigned to physic-sorbed water on Al_2O_3 or HSiW, while the last DTG peak located around 500 °C is similar to that of bulk HSiW and corresponds to decomposition of HSiW. No significant weight loss is observed above 550 °C. The results of $MoV/SiW/Al_2O_3$ catalyst are quite similar to that of SiW/Al_2O_3, indicating that the MoV part is stable and decomposition of HSiW before 500 °C.

The X-ray absorption spectra at W L_{III}-edge were measured to investigate the structure evolution of W species after heat treatment at different temperatures. W-containing components, HSiW or WO_x/Al_2O_3 (after calcination), act as solid acid to catalyse glycerol dehydration. The normalized XANES spectra (μ) and Fourier transform EXAFS are presented in Fig. 8 and 9, respectively. In Fig. 8, the absorption peaks are similar to each other and characteristic of W L_{III}-edge absorption deriving from electron transitions of $2p_{3/2}$

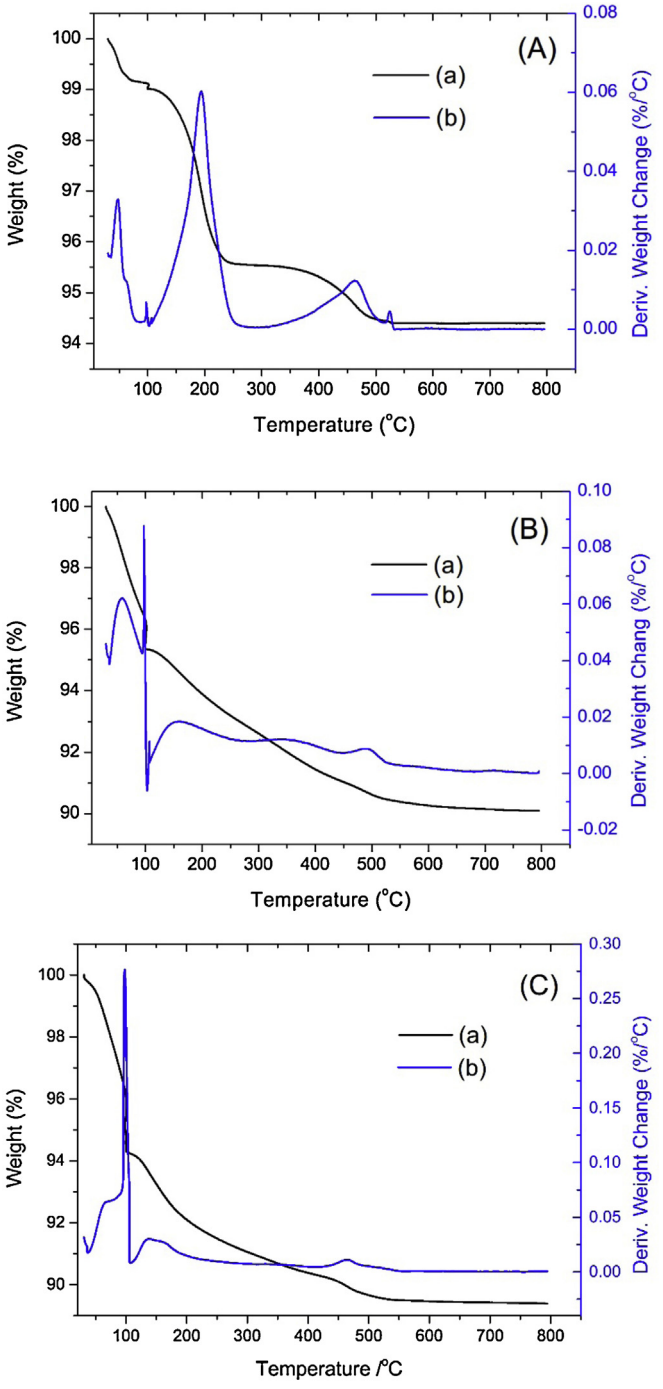

Fig. 7. TG (a) and DTG (b) plots for HSiW (A), SiW/Al_2O_3 (B) and $MoV/SiW/Al_2O_3$ (C).

state to a vacant 5d state [63–65]. The only one absorption peak is rather symmetry and no big difference is found in the first and second derivatives W L_{III}-edge XANES spectrum, suggesting the WO_x unit had no splitting of W 5d states due to ligand field [66]. From the k^3-Fourier transforms of EXAFS data of unsupported HSiW, the peaks at 1–2 Å, without phase-shift correction, is associated to the scattering from the nearest neighbor oxygen atoms, including shorter W=O – terminal oxygen (~1.7 Å) and longer W—O – bridging oxygen (~1.9 Å) [67]. The peaks at 3–4 Å arises from single and multiple scattering effects in W—O—W, even the contribution of oxygen atoms located in the third shell [67,68]. The supported SiW/Al_2O_3 shows some changes for peaks at 1–2 Å, which may

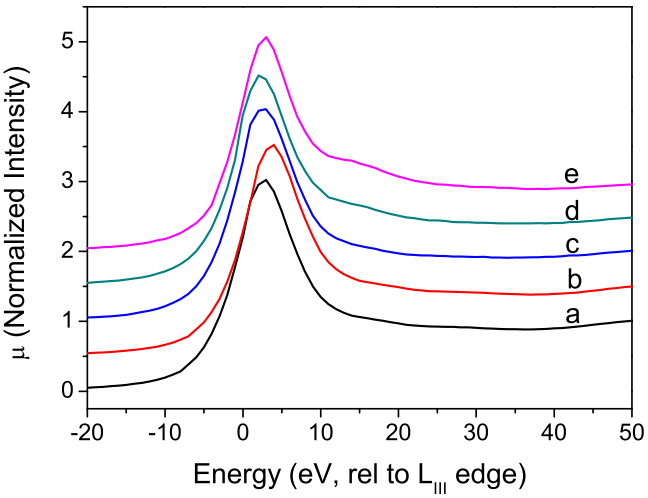

Fig. 8. The normalized W L_{III}-edge XANES data (μ) of (a) SiW/Al_2O_3 and MoV/SiW/Al_2O_3 calcined at (b) 350, (c) 450, (d) 550, and (e) 650 °C.

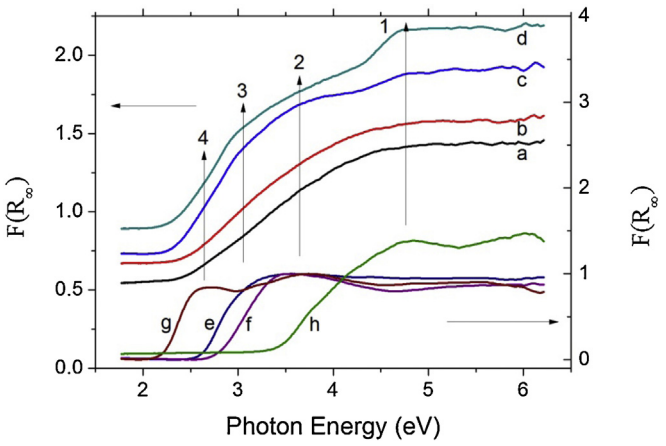

Fig. 10. UV–vis diffuse reflectance of MoV/SiW/Al_2O_3 catalysts calcined at (a) 350, (b) 450, (c) 550, (d) 650 °C and reference samples of (e) WO_3, (f)MoO_3, (g) V_2O_5, and (h) SiW/Al_2O_3.

be attributed to partial degradation of HSiW Keggin structure due to the basic properties of Al_2O_3, for example, loss of WO_6 fragment from $W_{12}O_{40}$ Keggin unit. But most of Keggin structure is still preserved because the peaks at 3–4 Å are similar to those of unsupported HSiW. The calcination of catalyst at 350 and 450 °C made further gradual evolution of peak shape at 1–2 Å, suggesting continuous degradation or even dissociation of the Keggin structure. Only one sharp peak is evolved after calcination at 550 and 650 °C and the scattering at 3–4 Å is disappeared. The Keggin structure was totally destroyed but the new structure was quite different from bulk WO_3 (Fig. 9g), that would be discussed in the following section.

The UV–vis diffuse reflectance spectra were shown in Fig. 10, including MoV/SiW/Al_2O_3 catalysts calcined at (a) 350, (b) 450, (c) 550, (d) 650 °C and (e) WO_3, (f) MoO_3, (g) V_2O_5, (h) SiW/Al_2O_3 as reference samples. Due to existence of various Mo/V/W-oxo-species in the catalysts, it is impossible to evolve all structures corresponding ligand to metal charge-transfer (LMCT) [69,70]. Therefore, only a few qualitative analyses are carried out. The MoV/SiW/Al_2O_3 catalysts calcined at 350 and 450 °C showed very similar absorption spectra. The absorption band in the region of 2.5–3.5 eV should arouse from Mo–V species, because W absorption band in the Keggin structure in SiW/Al_2O_3 starts from 3.5 eV. We also measured the UV–vis DR spectra of SiW/Al_2O_3 calcined at 350 and 450 °C, which showed very similar absorption bands too (not shown). The MoV/SiW/Al_2O_3 catalysts calcined at 550 and 650 °C showed obvious enhancement of absorption coefficients in some specific regions as indicated by up arrows. By referring the standard samples and XRD results, these increased absorptions are mainly assigned to, from high to low energy, molecular (isolated) four-coordinate W^{6+} centers tetrahedrally coordinated to oxygen ($O \rightarrow W^{6+}$) with edge energy value of 4.89 eV (1) [71], the bulk MoO_3 and/or WO_3 species (2 and 3) in 3.0–4.0 eV [72]. VO_x species such as V_2O_5 (4) in the region of less than 3.0 eV [73]. The contribution of MoO_3, WO_3 and V_2O_5 species to absorption will certainly extend to high energy region (>4.0 eV), but the absorption edge play important role to the appearance of the evident absorption band.

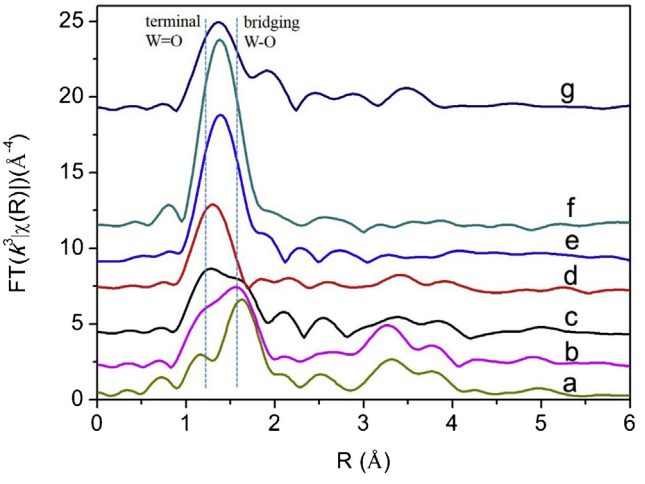

Fig. 9. The Fourier transform of W L_{III}-edge EXAFS (k^3, Δk = 0–11 Å^{-1}). (a) HSiW, (b)SiW/Al_2O_3, MoV/SiW/Al_2O_3 calcined at (c) 350, (d) 450, (e) 550, (f) 650 °C, and WO_3 (g).

4. Discussions

4.1. Reactivties and structure of supported species on catalysts

The 22.5% yield of acrolein and small amounts of other oxygenates (each lower than 10%) were generated from glycerol catalyzed by pure Al_2O_3. This is attributed to surface acidity of Al_2O_3, although the acidic density is much lower than tungstosilicic acid supported on Al_2O_3 (69 vs 283 μmol NH_3 g^{-1}-cat from NH_3-TPD). The acidic sites on Al_2O_3 were investigated previously and most of them were identified as Lewis acidic sites [61]. The higher surface area and pore volume of Al_2O_3 (187.2 m^2 g^{-1} and 0.251 cm^3 g^{-1} in present study) are also beneficial for the reaction. Al_2O_3 has been reported to be active in dehydration of glycerol to acrolein reaction in some publications [33,61,74].

Heteropolyacids (HPA) are a class of materials with well-defined structures and tunable acidity, making them excellent catalysts for acid–base reactions. HPA with stable Keggin structure has a general formula of $H_3MX_{12}O_{40}$, where M is the central atom (either P or Si) and X is the heteroatom (either W or Mo) [75,76]. The alumina or silica supported HPA catalysts have been applied to glycerol dehydration with thorough studies [30,33,56,57,59]. Among various HPAs supported on silica, $H_3SiW_{12}O_{40}/SiO_2$ showed the most stable catalytic activity in the dehydration of glycerol and was also resistant to water vapor [33,56]. In general, HPAs can be highly dispersed on alumina, silica and aluminosilicate supports [30,33,35,59,77]. In this work, we have synthesized HSiW supported on Al_2O_3 and obtained high dispersion of HSiW. In this sample, the Keggin

structure is well maintained according to our XRD, TEM and EXAFS analysis. Additionally, the BET surface area and pore volume of Al_2O_3 is decreased to 145.1 $m^2\ g^{-1}$ and 0.143 $cm^3\ g^{-1}$, respectively, after deposition of HSiW (Table 2). However, the dehydration activity is not influenced obviously. A 54.3% acrolein yield was produced on this SiW/Al_2O_3 catalyst, which is comparable with literature results from Atia et al. (58.9%) [59] and Kim et al. (44.1%) [56], but lower than that obtained on rubidium- or caesium-doped silicotungstic acid supported on alumina (87% or 88%) [35] for dehydration of glycerol under nitrogen atmosphere. Acetone is another major oxygenate product with 15.4% of selectivity. As stated above, the increase of acidic intensity, by loading of HSiW on Al_2O_3, could account for the improvement of acrolein yield through glycerol dehydration. For both Al_2O_3 and SiW/Al_2O_3 catalysts, the acid catalysis mechanism facilitates the formation of carbonium ion and subsequently a dihydroypropene structure, which might lead to acrolein by a further dehydration reaction (major reaction) and/or keto–enol tautomerism to 3-hydroxypropenal (side reaction in this case). A reverse aldol mechanism which converts 3-hydroxypropanal to acetaldehyde/formaldehyde and acetone happened under these conditions [57]. No acrylic acid or acetic acid produced on SiW/Al_2O_3 catalyst and only a very small amount of acetic acid formed on Al_2O_3. The SiW/Al_2O_3 catalyst produced a lower selectivity to CO_x than Al_2O_3 (7.8% vs 19.3%).

SiW/Al_2O_3 was further mixed with Mo_3VO_x oxides to prepare a series of $MoV/SiW/Al_2O_3$ catalysts which were applied to the one-step oxidative dehydration of glycerol to acrylic acid. All the $MoV/SiW/Al_2O_3$ catalysts were calcined in air before reaction. After calcination at 350 °C in air, the $MoV/SiW/Al_2O_3$ catalyst showed 12.1% of acrylic acid yield and 11.9% of acetic acid yield. The acrolein yield remained as low as 2.9%. Almost no other oxygenates was detected in the product because deep oxidation to CO and CO_2 happened. In the $MoV/SiW/Al_2O_3$ catalyst, Mo_3VO_x mixed oxides showed acicular structure which is common for the similar oxides materials [22]. The oxides were physically mixed with SiW/Al_2O_3 without particular interactions (TEM, Fig. 6b). The Mo_3VO_x acicular crystal, that composed of mixed oxides such as $(V_{0.07}Mo_{0.93})_5O_{14}$ at least, was found with low crystallinity by XRD and TEM observations. The $(V_{0.07}Mo_{0.93})_5O_{14}$ species are supposed to be active center for acrolein oxidation to acrylic acid because most acrolein converted and acrylic acid yield was high compared with catalyst calcined at higher temperature. The SiW/Al_2O_3 partially preserved its physicochemical property and HSiW Keggin structure, evidenced by coordination structure of neighbor atoms around center W atom (EXAFS) and high density of acidic sites on surface (TPD). And this is convinced because HSiW is stable below 400 °C observed in TG&DTG profiles (Fig. 7) [59]. Therefore, the sharp ammonium desorption peak at 420 °C may be aroused from well-defined Keggin units with abundant protonated H_3O^+ connections. The BET surface area decreased dramatically in comparison with SiW/Al_2O_3 (81.9 vs 145.1 $m^2\ g^{-1}$) due to the very low surface area of Mo_3VO_x oxides [78]. Actually, the N_2 adsorption-desorption isotherm of $MoV/SiW/Al_2O_3$ catalyst maintained the feature of that of SiW/Al_2O_3, suggesting similar porous structure to Al_2O_3.

Increasing calcination temperature to 450 °C led to better crystallinity of Mo_3VO_x mixed oxides. Isolate MoO_3 crystallites were identified besides the $(V,Mo)_2O_5$ and $(V_{0.07}Mo_{0.93})_5O_{14}$ species. Importantly, dissociation of Keggin structure of supported HSiW took place greatly, accompanying with the evolution of local coordination structure and surface acidic sites. The Keggin unit of HSiW is composed of 12 octahedral MO_6-units, which can be divided into 4 W_3O_{13} units. As a result, the whole structure has a tetrahedral symmetry. The W_3O_{13} unit would be the resulting species of dissociated of Keggin structure after calcination at 450 °C, because the two overlapped peaks amalgamated into one peak without much change of peak area in the range of 1–2 Å which represented the coordination oxygen atoms in the first shell, in W L_{III}-edge EXAFS in Fig. 9. The evolution of apparent two overlapped peaks suggested that the W—O bonds turned to flexible with similar bond distance. The fixed bond distances in the well-defined Keggin structure disappeared, such as the shorter W=O – terminal oxygen (~1.7 Å) and longer W—O – bridging oxygen (~1.9 Å). These W_3O_{13} species may bond to Al atoms on Al_2O_3 surface through W—O—Al interaction. Tungsten oxide-based materials comprise another class of solid acids, such as WO_x dispersed on Al_2O_3 or ZrO_2 with small and highly charged W^{+6} cations [71,79–81]. This can explain why high density of acidic sites (331 $\mu mol_{NH3}\ g^{-1}{}_{-cat}$) still exists after the catalyst was calcined at 450 °C and experienced HSiW dissociation. Therefore, acrolein yield still showed a little increase without loss of acrylic acid yield. More CO and CO_2 produced with higher O_2 conversion than the results on other catalysts. The appearance of MoO_3 species may account for the strong oxidation ability, because MoO_3 can be clearly identified only on this catalyst. MoO_3 has been reported in capable of catalyzing of total oxidation, such as soot combustion [82].

Further increasing calcination temperature to 550 °C and 650 °C induced continuous (crystal) structure changes of Mo_3VO_x and WO_x species in the catalysts. The MoO_3 species that observed in sample calcined at 450 °C disappeared and were replaced by a number of complicated hetero-polyoxo-Mo/V agglomerates, such as Mo_4O_{11}, V_2O_5, VO_2, even eutectic $(V,Mo)_2O_5$ and $(V,Mo)_4O_{11}$. The WO_x species, come from the dissociation of HSiW, evolved to two different forms. One is WO_3 nanoclusters which can be detected by XRD, the other is WO_4 units highly dispersed on the surface of Al_2O_3 or Mo_3VO_x mixed oxide crystals with strong interactions (coordination). The structure evolution of the catalyst calcined at different temperatures is shown in Fig. 11. The WO_4 unit structure was deduced from EXAFS. Only one distinct peak with high area is shown in R = 1–2 Å, suggesting that single oxygen shell is dominant for WO_x species. The catalysts calcined at 550 and 650 °C had similar local structure for Mo/V/W oxides. The difference is that bigger crystal size was obtained with catalyst calcined at 650 °C. Moreover, the mesoporous structure of Al_2O_3 was destroyed or severely blocked. Therefore, the surface area became very low. This leads to both acrolein and acrylic acid yield decrease compared with catalyst calcined at 550 °C. For $MoV/SiW/Al_2O_3$ catalyst calcined at 550 °C, the acrolein yield has a bit higher value of 15% while acrylic acid yield dropped. This may be attributed to the disappearance of highly active species, such as $(V_{0.07}Mo_{0.93})_5O_{14}$, and acrolein cannot convert to acrylic acid efficiently.

4.2. Reaction pathways and active species

As glycerol possesses two, secondary or primary, different hydroxyl radicals, the dehydration can take place at either radical and produce two parallel products, 3-hydrxypropionaldehyde (3-HPA) and acetol, respectively [33,83]. 3-HPA is very unstable and easily dehydrated to acrolein. Actually, both 3-HPA and acetol are very reactive and second reactions, i.e., condensation and oligomerization, can take place to form higher molecular weight oxygenates on the surface that can block the active sites. Meanwhile, 3-HPA and acetol are believed to be major sources of CO_x production, although acrolein and other hydrocarbon intermediates, even the final products of acrylic acid and acetic acid, can all be oxidized to CO_x. Corma et al. investigated the product selectivity in the conversion of several main products obtained from glycerol processing [84], and concluded that acetol could produce more CO_x than other reactants fed. Our recent results also showed the same conclusion that larger amount of CO_x could be formed from acetol than acrolein, acrylic acid and acetic acid on a MoV-based mixed oxides catalyst (not published). When the catalyst was separated to dehydration and oxidation catalyst and run in the double bed

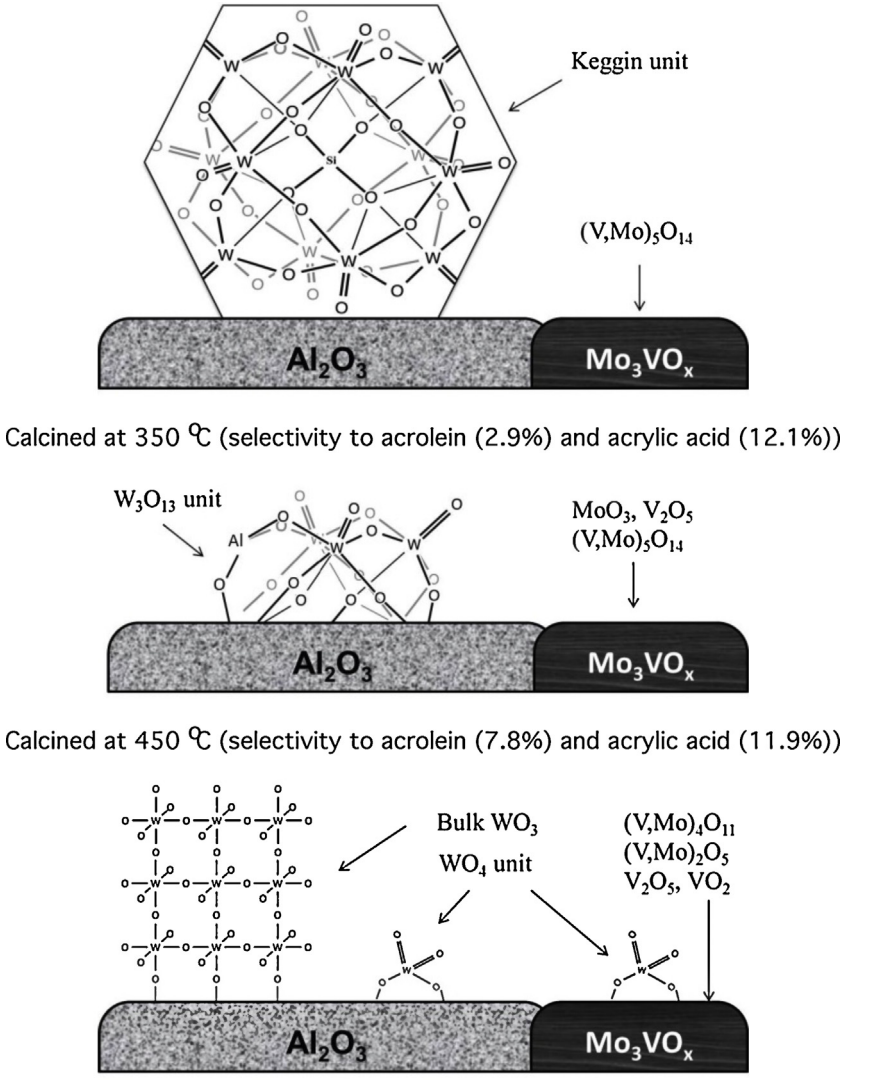

Fig. 11. Scheme of structure evolution of supported species with different calcination temperature.

configuration, the yield to acrylic acid was improved while yields to CO and CO_2 decreased significantly, as compared with the one-step reaction. These results indicate that the deep oxidation of acrolein is not serious enough to produce much CO_x. Therefore, some intermediates, like 3-HPA, must be responsible for the deep oxidation in the one-step reaction, as they are easily accessible to access (V, Mo)O_x species in MoV/SiW/Al_2O_3 catalyst in the one step reaction. However, it could complete the conversion to acrolein by dehydration reaction in double bed and avoid oxidizing to CO_x, because it has no chance to contact with V–Mo oxides species.

Acrylic acid is undoubtedly produced from acrolein by partial oxidation. The experiment showed that acetic acid was also produced in parallel with acrylic acid over catalysts calcined at 350 °C (Fig. 1). Acetic acid comes from partial oxidation of acetaldehyde, which is generated by cracking reaction of two intermediates of pyruvaldehyde and acetone. Acetone can be made by dehydration of propanediol, while pyruvaldehyde and propanediol are produced by H-transfer reaction of acetol, including dehydrogenation to pyruvaldehyde and hydrogenation to propanediol. The proposed reaction pathway is shown in Fig. 12.

The (V,Mo)$_5O_{14}$ crystallines, especially ($V_{0.07}Mo_{0.93}$)$_5O_{14}$, are the active species in oxidation of acrolein to acrylic acid in present bifunctional catalyst especially. This is similar to Ovsiser et al.'s conclusion because they found (MoVW)$_5O_{14}$ phase was in majority in the active and selective catalysts for acrolein oxidation to acrylic acid [58]. Although the commercial catalysts for acetaldehyde oxidation to acetic acid are manganese acetate or cobalt acetate, V–Mo oxides could also catalyze this reaction efficiently. For example, acetaldehyde could be oxidized to acetic acid with selectivity up to 82% at ~200 °C over VO_x catalyst [85]. This may explain why yield to acetic acid remains a constant around 12% on various MoV/SiW/Al_2O_3 catalysts with either different Mo_3VO_x contents or calcination temperatures. The MoO_3 crystallines, which were detected in the catalyst calcined at 450 °C, have strong oxidation ability to promote total oxidation to CO_x [86,87], therefore much higher CO_x selectivity and O_2 conversion were observed on this catalyst (Fig. 2). The increase of acrolein selectivity and drop of acrylic acid selectivity on catalyst calcined at 550 °C is attributed to the disappearance of active (V, Mo)$_5O_{14}$ crystallines after calcination. Certainly, decline of surface area of active components

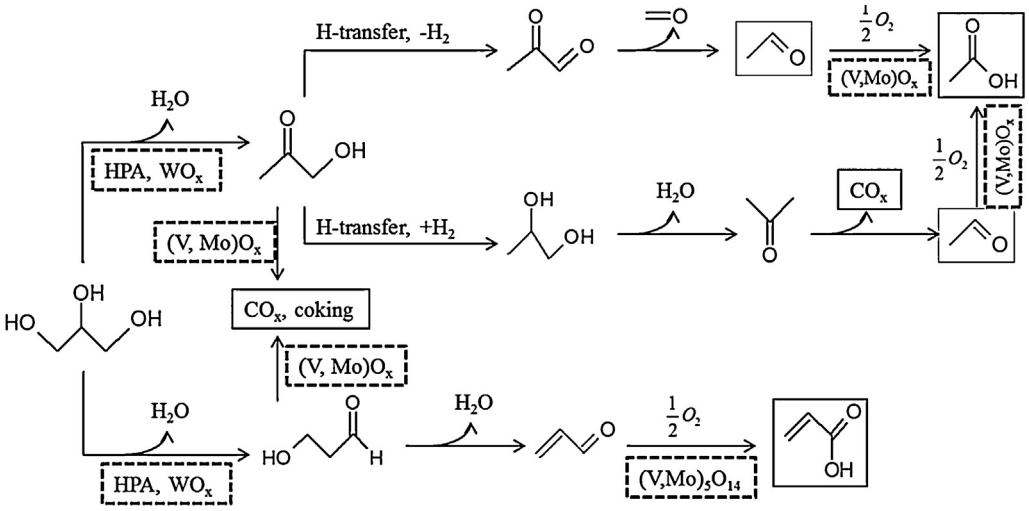

Fig. 12. Proposed reaction pathways for one-step conversion of glycerol over MoV/SiW/Al_2O_3 catalysts.

and pore structure loss may also contribute to the changes. This is more credible for catalyst calcined at 650 °C, which resulted in both acrolein and acrylic acid selectivity drop. The mechanically mixed Mo_3VO_x (450 °C) and $H_4SiW_{12}O_{40}/Al_2O_3$ catalyst did not show higher acrylic acid than the bifunctional catalyst, suggesting the easy access of intermediates to V–Mo species causing deep oxidation was not avoided in this manner.

In summary, the deep oxidation to CO_x on (V, Mo)O_x species is the main obstacle to achieve high acrylic acid in the one-step conversion of glycerol, because some reaction intermediates, such as acetol and 3-HPA, are very easy to be combusted on active V–Mo–O species. The further development of bifunctional catalyst for one-step conversion of glycerol to acrylic acid may focus on improving two internal selectivities. One is glycerol dehydration to 3-HPA selectivity, the other one is 3-HPA dehydration to acrolein selectivity. To improve dehydration and inhibit oxidation of 3-HPA seems more crucial because selectivity of 3-HPA from glycerol is usually higher demonstrated by the high selectivity of acrolein over dehydration catalyst. The following guidelines are proposed for future catalyst development, (1) isolation of dehydration active sites with oxidation sites with appropriate distance, to avoid easy occurrence of 3-HPA oxidation; (2) enhancement of reaction velocity of 3-HPA dehydration versus oxidation to improve selectivity towards acrolein than CO_x and other oxidation products; (3) adjustment of crystal phase composition of V–Mo–O mixed oxides to make more active species available for acrolein oxidation.

5. Conclusions

Acrylic acid is produced in one-step conversion of glycerol over $Mo_3VO_x/H_4SiW_{12}O_{40}/Al_2O_3$ catalysts. It is found that acetic acid is generated in parallel with acrylic acid with similar yield while the acrolein yield is rather low for catalysts calcined at 350 °C. Calcination of $Mo_3VO_x/H_4SiW_{12}O_{40}/Al_2O_3$ catalyst with increasing temperature leads to structure evolution of the supported active species and subsequent activity change. $(V_{0.07}Mo_{0.93})_5O_{14}$ crystallines are observed on catalyst calcined at 350 °C. MoO_3 and $(V_{0.07}Mo_{0.93})_5O_{14}$ crystallines appear in the catalyst calcined at 450 °C, and more crystal polyoxo compounds formed in the catalysts calcined at 550 and 650 °C. $H_4SiW_{12}O_{40}$ begins to lose its Kiggin structure at 450 °C, and supported WO_x species continue to work as active centers for glycerol dehydration. The $(V_{0.07}Mo_{0.93})_5O_{14}$ crystallines should be the most active species for acrolein oxidation to acrylic acid. The deep oxidation to CO_x of some reaction intermediates, such as acetol and 3-hydrxypropionaldehyde, is the main reason for low yield of acrylic acid.

Acknowledgement

Funding from the Science and Engineering Research Council (SERC), Singapore Agency for Science, Technology and Research (A*STAR), grant no. 1124004024, in support of this project is gratefully acknowledged.

Appendix A. Supplementary data

Supplementary data associated with this article can be found, in the online version, at http://dx.doi.org/10.1016/j.apcatb.2015.02.032.

References

[1] S. Abad, X. Turon, Biotechnol. Adv. 30 (2012) 733–741.
[2] J.R. Almeida, L.C. Favaro, B. Quirino, Biotechnol. Biofuels 5 (2012) 48.
[3] A. Andre, A. Chatzifragkou, P. Diamantopoulou, D. Sarris, A. Philippoussis, M. Galiotou-Panayotou, M. Komaitis, S. Papanikolaou, Eng. Life Sci. 9 (2009) 468–478.
[4] A. Leoneti, V. Aragao-Leoneti, S. de Oliveira, Renew. Energy 45 (2012) 138–145.
[5] B. Katryniok, S. Paul, V. Bellière-Baca, P. Rey, F. Dumeignil, Green Chem. 12 (2010) 2079.
[6] D.Y.C. Leung, X. Wu, M.K.H. Leung, Appl. Energy 87 (2010) 1083–1095.
[7] B. Katryniok, S. Paul, M. Capron, C. Lancelot, V. Bellière-Baca, P. Rey, F. Dumeignil, Green Chem. 12 (2010) 1922.
[8] J. Chaminand, L.A. Djakovitch, P. Gallezot, P. Marion, C. Pinel, C.C. Rosier, Green Chem. 6 (2004) 359.
[9] Y. Feng, H. Yin, A. Wang, L. Shen, L. Yu, T. Jiang, Chem. Eng. J. 168 (2011) 403–412.
[10] L. Gong, Y. Lu, Y. Ding, R. Lin, J. Li, W. Dong, T. Wang, W. Chen, Appl. Catal. A: Gen. 390 (2010) 119–126.
[11] P.D. Vaidya, A.E. Rodrigues, Chem. Eng. Technol. 32 (2009) 1463–1469.
[12] G. Wen, Y. Xu, H. Ma, Z. Xu, Z. Tian, Int. J. Hydrogen Energy 33 (2008) 6657–6666.
[13] A.O. Menezes, M.T. Rodrigues, A. Zimmaro, L.E.P. Borges, M.A. Fraga, Renew. Energy 36 (2011) 595–599.
[14] N. Kondamudi, M. Misra, S. Banerjee, S. Mohapatra, S. Mohapatra, Appl. Catal. B: Environ. 126 (2012) 180–185.
[15] T. Roncal, C. Muñoz, L. Lorenzo, B. Maestro, M.D.M. Díaz de Guereñu, Enzyme Microb. Technol. 50 (2012) 143–150.
[16] S. Gil, M. Marchena, L. Sánchez-Silva, A. Romero, P. Sánchez, J.L. Valverde, Chem. Eng. J. 178 (2011) 423–435.
[17] H. Mori, A.H.E. Müller, Prog. Polym. Sci. 28 (2003) 1403–1439.
[18] K.R.M. Vidts, B. Dervaux, F.E. Du Prez, Polymer. 47 (2006) 6028–6037.
[19] G. Mestl, Top. Catal. 38 (2006) 69–82.

[20] U. Cremer, M. Dieterle, S. Jourdan, J. Petzoldt, K.J. Muller-Engel, in: U.S.P.A.T. Office (Ed.), Assignee: BASF Aktiengesellschaft, US Patent (US 2005/0272952 A1), United States.
[21] L. Giebeler, P. Kampe, A. Wirth, A.H. Adams, J. Kunert, H. Fuess, H. Vogel, J. Mol. Catal. A: Chem. 259 (2006) 309–318.
[22] J. Deleplanque, J.L. Dubois, J.F. Devaux, W. Ueda, Catal. Today 157 (2010) 351–358.
[23] F. Wang, J.-L. Dubois, W. Ueda, J. Catal. 268 (2009) 260–267.
[24] F. Wang, J.-L. Dubois, W. Ueda, Appl. Catal. A: Gen. 376 (2010) 25–32.
[25] A.S. de Oliveira, S.J.S. Vasconcelos, J.R. de Sousa, F.F. de Sousa, J.M. Filho, A.C. Oliveira, Chem. Eng. J. 168 (2011) 765–774.
[26] A. Ulgen, W.F. Hoelderich, Appl. Catal. A: Gen. 400 (2011) 34–38.
[27] P. Lauriol-Garbey, S. Loridant, V. Bellière-Baca, P. Rey, J.-M.M. Millet, Catal. Commun. 16 (2011) 170–174.
[28] N.R. Shiju, D.R. Brown, K. Wilson, G. Rothenberg, Top. Catal. 53 (2010) 1217–1223.
[29] S. Erfle, U. Armbruster, U. Bentrup, A. Martin, A. Brückner, Appl. Catal. A: Gen. 391 (2011) 102–109.
[30] H. Atia, U. Armbruster, A. Martin, Appl. Catal. A: Gen. 393 (2011) 331–339.
[31] W. Yan, G.J. Suppes, Ind. Eng. Chem. Res. 48 (2009) 3279–3283.
[32] P. Lauriol-Garbey, J.M.M. Millet, S. Loridant, V. Bellière-Baca, P. Rey, J. Catal. 281 (2011) 362–370.
[33] E. Tsukuda, S. Sato, R. Takahashi, T. Sodesawa, Catal. Commun. 8 (2007) 1349–1353.
[34] Q. Liu, Z. Zhang, Y. Du, J. Li, X. Yang, Catal. Lett. 127 (2008) 419–428.
[35] M.H. Haider, N.F. Dummer, D. Zhang, P. Miedziak, T.E. Davies, S.H. Taylor, D.J. Willock, D.W. Knight, D. Chadwick, G.J. Hutchings, J. Catal. 286 (2012) 206–213.
[36] L. Yang, J.B. Joo, N.D. Kim, K.S. Jung, J. Yi, Kor. J. Chem. Eng. 27 (2010) 1695–1699.
[37] C.-J. Jia, Y. Liu, W. Schmidt, A.-H. Lu, F. Schüth, J. Catal. 269 (2010) 71–79.
[38] E. Kraleva, R. Palcheva, L. Dimitrov, U. Armbruster, A. Brückner, A. Spojakina, J. Mater. Sci. 46 (2011) 7160–7168.
[39] L.-Z. Tao, S.-H. Chai, Y. Zuo, W.-T. Zheng, Y. Liang, B.-Q. Xu, Catal. Today 158 (2010) 310–316.
[40] L.-Z. Tao, B. Yan, Y. Liang, B.-Q. Xu, Green Chem. 15 (2013) 696.
[41] S. Chai, H. Wang, Y. Liang, B. Xu, J. Catal. 250 (2007) 342–349.
[42] F. Cavani, S. Guidetti, L. Marinelli, M. Piccinini, E. Ghedini, M. Signoretto, Appl. Catal. B: Environ. 100 (2010) 197–204.
[43] F. Cavani, S. Guidetti, C. Trevisanut, E. Ghedini, M. Signoretto, Appl. Catal. A: Gen. 409–410 (2011) 267–278.
[44] M. Massa, A. Andersson, E. Finocchio, G. Busca, J. Catal. 307 (2013) 170–184.
[45] M. Massa, A. Andersson, E. Finocchio, G. Busca, F. Lenrick, L.R. Wallenberg, J. Catal. 297 (2013) 93–109.
[46] K. Omata, S. Izumi, T. Murayama, W. Ueda, Catal. Today 201 (2013) 7–11.
[47] A. Drochner, P. Kampe, J. Kunert, J. Ott, H. Vogel, Appl. Catal. A: Gen. 289 (2005) 74–83.
[48] S. Endres, P. Kampe, J. Kunert, A. Drochner, H. Vogel, Appl. Catal. A: Gen. 325 (2007) 237–243.
[49] T. Jekewitz, N. Blickhan, S. Endres, A. Drochner, H. Vogel, Catal. Commun. 20 (2012) 25–28.
[50] J. Kunert, A. Drochner, J. Ott, H. Vogel, H. Fueß, Appl. Catal. A: Gen. 269 (2004) 53–61.
[51] M.D. Soriano, P. Concepción, J.M.L. Nieto, F. Cavani, S. Guidetti, C. Trevisanut, Green Chem. 13 (2011) 2954.
[52] F. Wang, J. Xu, J.-L. Dubois, W. Ueda, ChemSusChem. 3 (2010) 1383–1389.
[53] A. Chieregato, F. Basile, P. Concepción, S. Guidetti, G. Liosi, M.D. Soriano, C. Trevisanut, F. Cavani, J.M.L. Nieto, Catal. Today 197 (2012) 58–65.
[54] A. Chieregato, M.D. Soriano, F. Basile, G. Liosi, S. Zamora, P. Concepción, F. Cavani, J.M. López Nieto, Appl. Catal. B: Environ. 150–151 (2014) 37–46.
[55] R. Liu, T. Wang, D. Cai, Y. Jin, Ind. Eng. Chem. Res. 53 (2014) 8667–8674.
[56] Y.-T. Kim, K.-D. Jung, E.-D. Park, B. Kor, Chem. Soc. 31 (2010) 3283–3290.
[57] L. Cheng, X.P. Ye, Catal. Lett. 130 (2009) 100–107.
[58] O. Ovsitser, Y. Uchida, G. Mestl, G. Weinberg, A. Blume, J. Jäger, M. Dieterle, H. Hibst, R. Schlögl, J. Mol. Catal. A: Chem. 185 (2002) 291–303.
[59] H. Atia, U. Armbruster, A. Martin, J. Catal. 258 (2008) 71–82.
[60] L. Giebeler, A. Wirth, J.A. Martens, H. Vogel, H. Fuess, Appl. Catal. A: Gen. 379 (2010) 155–165.
[61] Y.T. Kim, K.-D. Jung, E.D. Park, Appl. Catal. B: Environ. 107 (2011) 177–187.
[62] L.R. Pizzio, M.N. Blanco, Micropor. Mesopor. Mater. 103 (2007) 40–47.
[63] A. Kubacka, R. Si, P. Michorczyk, A. Martínez-Arias, W. Xu, J.C. Hanson, J.A. Rodriguez, M. Fernández-García, Appl. Catal. B: Environ. 132–133 (2013) 423–432.
[64] M. Fernández-García, A. Martínez-Arias, A. Fuerte, J.C. Conesa, J. Phys. Chem. B 109 (2005) 6075–6083.
[65] F. Hilbrig, H.E. Goebel, H. Knoezinger, H. Schmelz, B. Lengeler, J. Phys. Chem. 95 (1991) 6973–6978.
[66] S. Yamazoe, Y. Hitomi, T. Shishido, T. Tanaka, J. Phys. Chem. C 112 (2008) 6869–6879.
[67] E. Burattini, Jpn. J. Appl. Phys. 32 (1993) 655–657.
[68] C. Martıín, G. Solana, P. Malet, V. Rives, Catal. Today 78 (2003) 365–376.
[69] M.H. Youn, H. Kim, J.C. Jung, I.K. Song, K.P. Barteau, M.A. Barteau, J. Mol. Catal. A: Chem. 241 (2005) 227–232.
[70] Y.-M. Liu, Y. Cao, N. Yi, W.-L. Feng, W.-L. Dai, S.-R. Yan, H.-Y. He, K.-N. Fan, J. Catal. 224 (2004) 417–428.
[71] D.G. Barton, M. Shtein, R.D. Wilson, S.L. Soled, E. Iglesia, J. Phys. Chem. B 103 (1999) 630–640.
[72] P.V.D. Voort, M.G. White, M.B. Mitchell, A.A. Verberckmoes, E.F. Vansant, Spectrochim. Acta Part A 53 (1997) 2181–2187.
[73] R. Bulánek, P. Čičmanec, M. Setnička, Phys. Procedia 44 (2013) 195–205.
[74] Y.T. Kim, K.-D. Jung, E.D. Park, Appl. Catal. A: Gen. 393 (2011) 275–287.
[75] I. Kozhevnikov, Handbook of Green Chemistry, Wiley-VCH Verlag GmbH & Co., KGaA, 2010.
[76] I.V. Kozhevnikov, Chem. Rev. 98 (1998) 171–198.
[77] A.D. Newman, D.R. Brown, P. Siril, A.F. Lee, K. Wilson, Phys. Chem. Chem. Phys. 8 (2006) 2893.
[78] D. Vitry, Appl. Catal. A: Gen. 251 (2003) 411–424.
[79] D.G. Barton, S.L. Soled, G.D. Meitzner, G.A. Fuentes, E. Iglesia, J. Catal. 181 (1999) 57–72.
[80] S.L. Soled, G.B. McVicker, L.L. Murrell, L.G. Sherman, N.C. Dispenziere Jr., S.L. Hsu, D. Waldman, J. Catal. 111 (1988) 286–295.
[81] R. Zhang, J. Jagiello, J.F. Hu, Z.Q. Huang, J.A. Schwarz, A. Datye, Appl. Catal. A: Gen. 84 (1992) 123–139.
[82] M.A. Hasan, M.I. Zaki, K. Kumari, L. Pasupulety, Thermochim. Acta 320 (1998) 23–32.
[83] A. Witsuthammakul, T. Sooknoi, Appl. Catal. A: Gen. 413–414 (2012) 109–116.
[84] A. Corma, G. Huber, L. Sauvanaud, P. O' Connor, J. Catal. 257 (2008) 163–171.
[85] W.Y. Suprun, D. Kießling, T. Machold, H. Papp, Chem. Eng. Technol. 29 (2006) 1376–1380.
[86] T. Ressler, A. Walter, Z.D. Huang, W. Bensch, J. Catal. 254 (2008) 170–179.
[87] K. Chen, E. Iglesia, A.T. Bell, Studies in Surface Science and Catalysis, in: J.J.S.E. Iglesia, T.H. Fleisch (Eds.), Elsevier, 2010, pp. 507–512.